Effect on chlorine incorporation as Mg is alloyed into ZnSe

Yaxiang Yang, Brenda VanMil, Leonid Muratov, Bernard R. Cooper, and Thomas H. Myers
West Virginia University, Department of Physics, Morgantown, West Virginia 26506-6315

John M. Wills
Theory Division, Los Alamos National Laboratory, Los Alamos, New Mexico 87545
(Received 11 January 2002; revised manuscript received 10 May 2002; published 31 October 2002)

We have investigated chlorine incorporation in ZnSe and $Zn_xMg_{1-x}Se$ through both modeling and experiment. Solubility issues, native defects and chlorine-impurity-related defects have been studied using the *ab initio* full potential linear muffin-tin-orbital method. Our calculations indicate that the addition of Mg reduces the formation energy for chlorine on the Se site, thereby predicting increased solubility. Subsequent chlorine doping experiments in $Zn_xMg_{1-x}Se$ using molecular beam epitaxy indicated significantly higher chlorine incorporation in the presence of magnesium, directly supporting the prediction of the calculations. Calculations support the strong tendency for the formation of a defect complex between a chlorine impurity at the Se site and a vacancy at the neighboring Zn site for heavy *n*-type doping. The formation of this defect serves to compensate, i.e., negate, the chlorine as an *n*-type dopant. Experimental observations indicated that significant compensation occurs for heavy Cl doping. There are competing mechanisms that contribute to the effect of magnesium on chlorine when used as an *n*-type dopant in ZnSe. First, the formation energies for chlorine substituting for selenium decrease in the presence of magnesium. Second, the formation energies of the Cl_{Se}-V_{Zn} complex also decrease. Finally, the band gap increases in the presence of magnesium, decreasing the net electron concentration at room temperature. Thus, the net effect of adding magnesium is to *decrease* the maximum achievable carrier concentration through the use of chlorine as an *n*-type dopant.

DOI: 10.1103/PhysRevB.66.165222 PACS number(s): 61.72.Bb, 61.72.Ji, 61.72.Vv

I. INTRODUCTION

The wide-band-gap semiconductor ZnSe and its alloy $Zn_xMg_{1-x}Se$ are of active interest for potential electrooptic applications. This materials system can be used for devices operating in the blue to ultraviolet spectral region. While GaN and its alloys are currently more commercially viable for these efforts,[1] the ZnSe alloy system continues to be of interest. In the literature, the role of defects and defect complexes in ZnSe with *n*-type and *p*-type doping has been repeatedly addressed.[2–9] Many of these defects can act as compensating centers reducing the maximum achievable carrier concentration. In the case of chlorine doping in ZnSe, theoretical results[7] have indicated that the substitutional-chlorine-zinc-vacancy complex is the most probable candidate for the compensating center. Using positron annihilation experiments, Saarinen *et al.*[10] recently identified zinc vacancies in *n*-type ZnSe:Cl. The defect complex Cl_{Se}-V_{Zn} has been suggested to be formed in heavily Cl-doped ZnSe.[11,12] Indeed, Akimoto *et al.*[12] suggested that the concentration of the zinc-vacancy is of the same order of magnitude as that of four-coordinated Cl which is incorporated in the Se lattice site.

The addition of magnesium to form $Zn_xMg_{1-x}Se$ increases the bandgap, lowers the index of refraction,[13] and allows tailoring of the lattice constant. These effects make $Zn_xMg_{1-x}Se$ attractive for heterostructure devices where optical or electrical confinement is desired. Calculations by Okuyama *et al.*[14] showed an increase of band gap in $Zn_xMg_{1-x}Se$ from 2.6 eV for ZnSe to 3.7 eV for MgSe (in zinc blende structure) in close agreement with their quoted experimental values of 2.7 and 3.6 eV, respectively. Chlorine, as the most successful *n*-type dopant in ZnSe, is also the best candidate for *n*-type doping in ZnMgSe. However, experimental results have been disappointing. The data by Ferreira *et al.*[15] indicate that the highest electron concentration decreases with increasing Mg content in ZnMgSe. In particular, they suggest that the chlorine's solubility is lowered by the addition of Mg. Therefore, to gain an understanding of the issues involved, we used the *ab initio* full potential linear muffin-tin-orbital method to model native defects and chlorine-related defects in ZnSe and $Zn_xMg_{1-x}Se$. We focused on the relative changes in the electronic properties with increasing Mg content, and our theoretical results are compared with our own most recent experimental results as well as previous work.

II. COMPUTATIONAL APPROACH

A. FP-LMTO method

An *ab initio* full-potential linear combination of muffin-tin orbitals (FP-LMTO) method, including a force routine,[16–20] was used for this calculation. The electron exchange-correlation was treated in the local-density approximation (LDA) with the Ceperly-Alder[21] exchange-correlation function parametrized by Perdew and Zunger.[22] Atomic forces were calculated using the Hellman-Feynman theorem.[23] Detailed information about this method can be found in Refs. 16–20 and 24.

In all calculations reported in this paper, zinc $3d$ electrons were treated as valence electrons, while Se $3d$ electrons were included in the core. Four to six wave number parameters (κ's[16–20]) were used, that is two common κ's for all the elements and an individual one for each element. For an orbital with a given angular momentum, each κ creates its

own subset of basis functions. Two orbitals with the same angular momentum but with a different principal quantum number are included by placing them in different energy windows. As a result, eleven to twenty-three muffin-tin-orbital basis functions in two energy windows were used for each Mg, Zn, Se, and Cl atom. Scalar relativistic corrections were included, but not spin-orbit coupling. For the charged defects, a neutralizing uniform background charge was used to avoid long-range Coulomb interactions. To account for the effect of the background charge on the formation energies, we applied a monopole correction (energy of a lattice of point charges immersed in neutralizing jelium) $e^2Q^2\alpha/L\epsilon$, where Q is the charge of the defect, α is the Madelung constant, ϵ is the dielectric constant, and L is a lattice constant of the supercell.[24] For example, the magnitude of this correction is 0.27 eV for the singly charged chlorine substitution for selenium $(Cl_{Se})^{1+}$. This correction affects only the absolute values of the formation energies and does not change the dependence on magnesium concentration. Because of this, and the fact that other corrections are much smaller, for the present publication we restrict ourselves to this term only. We also neglected changes related to variation of ϵ.

Most of our calculations were performed using a 32-atom supercell. Different concentrations of Mg were achieved by substituting one, two, or three Zn atoms with Mg atoms in this 32-atom supercell. Thus, three ZnMgSe alloys $Zn_{0.94}Mg_{0.06}Se$, $Zn_{0.87}Mg_{0.13}Se$, $Zn_{0.81}Mg_{0.19}Se$, and pure ZnSe were considered. Lattice relaxation around the defects has been shown to be significant for ZnSe in previous work.[3,7,8,25] This is even more important for the present calculation since the differences among the formation energies of the same defect in $Zn_xMg_{1-x}Se$ is very small for different Mg content. Therefore, we consider lattice relaxation around defects for most cases presented here.

In order to minimize the numerical discrepancy, all calculations for a material have been performed using supercells with identical symmetry and the same k points in the Brillouin zone. In this approach, most of the numerical errors associated with the limited sampling of the Brillouin zone cancel each other. Tests were performed to insure that the size of the supercell and number of k points do not affect the final results.

B. Formation energy of defects

In the calculation of the defect formation energy, one has to compare the total energy for a supercell with a defect and the total energy for the corresponding perfect supercell. Formation energy E^f of the defect of type D^n with charge n is calculated as

$$E^f = \mathrm{TE}_{\mathrm{defect}} + \mu_{\mathrm{defect}} + n\mu_e - \mathrm{TE}_{\mathrm{perfect}},$$

where $\mathrm{TE}_{\mathrm{defect}}$ is the total energy of a supercell with a defect, $\mathrm{TE}_{\mathrm{perfect}}$ is the total energy of a corresponding perfect supercell, μ_e is the electron chemical potential (Fermi level) measured with respect to the valence-band maximum, and μ_{defect} is the change in chemical potential due to removing or substituting atoms necessary to form a defect. This change can be expressed as:

TABLE I. Defect formation energy of Cl^{1+}_{Se} and Cl^{0}_{Se} in ZnSe for 32-atom and 64-atom supercell with the energies given in eV. The calculated value for the heat of formation (ΔH) is 1.4 eV for ZnSe.

Defect (Cell Size)	Formation Energy
$(Cl_{Se})^0$ (32)	$1.36+\lambda\Delta H$
$(Cl_{Se})^0$ (64)	$1.32+\lambda\Delta H$
$(Cl_{Se})^{1+}$ (32)	$-0.59+\lambda\Delta H+\mu_e$
$(Cl_{Se})^{1+}$ (64)	$-0.62+\lambda\Delta H+\mu_e$

$$\mu_{\mathrm{defect}} = \begin{cases} \mu_{\mathrm{Se}} - \mu_{\mathrm{Cl}} & \text{for } Cl_{Se}, \\ \mu_{\mathrm{ZnSe}} - \mu_{\mathrm{Cl}} & \text{for } Cl_{Se} - V_{Zn}, \\ \mu_{\mathrm{Zn}} & \text{for } V_{Zn}, \end{cases}$$

where μ_{Se}, μ_{Zn}, μ_{Cl}, and μ_{ZnSe} are the chemical potentials of the Se, Zn, Cl atoms, and ZnSe pair in ZnSe. In turn, μ_{Se}, μ_{Zn}, and μ_{ZnSe} can be obtained as

$$\mu_{\mathrm{Se}} = \mu^{\mathrm{bulk}}_{\mathrm{Se}} - \lambda\Delta H, \mu_{\mathrm{Zn}} = \mu^{\mathrm{bulk}}_{\mathrm{Zn}} - (1-\lambda)\Delta H,$$

$$\mu_{\mathrm{Se}} + \mu_{\mathrm{Zn}} = \mu_{\mathrm{ZnSe}} = \mu^{\mathrm{bulk}}_{\mathrm{Se}} + \mu^{bulk}_{\mathrm{Zn}} - \Delta H,$$

where ΔH is the heat of formation of ZnSe, parameter λ varies from 0 to 1, $\lambda=0$ for Zn rich, and $\lambda=1$ for Se rich. For the chemical potential of a chlorine atom (μ_{Cl}), we used the total energy of a single isolated chlorine atom. This omits effects of the solid state environment on the chlorine atom. In addition, the LDA calculations with the Ceperly-Alder[21] exchange-correlation function parametrized by Perdew and Zunger[22] (as used for the rest of the calculation) were not designed for use on isolated atoms. Therefore, there may be a significant computational error associated with μ_{Cl}. However, this error can only affect absolute values, while the differences between formation energies as presented in Table II are still reliable.

The density functional theory (DFT) is designed only to accurately calculate the total energy and charge density for the ground state of matter. As such, DFT usually underestimates the band gap by a factor of two. For example, for ZnSe the calculated band gap is 1.2 eV (present calculations) in comparison with the experimental value of about 2.6 eV. Despite this fact, it is commonly accepted that the dispersion of valence and conduction bands are calculated quite accurately in the framework of DFT. This statement has been supported not only by the ability of DFT to explain experimental observations but also by calculations that include many-body corrections (e.g., Refs. 26, 27). In this publication, we will follow the standard approach and increase the band gap to its experimental values. The fact that we are using our calculations to understand trends due to the addition of magnesium relies more on the ability to calculate the dispersion of the levels rather than the absolute magnitude.

To study the effects of the size of the supercell on results, we compare the formation energy of Cl^{1+}_{Se} and Cl^{0}_{Se} in both a 32-atom supercell and a 64-atom supercell in Table I. The energy difference for two different supercell sizes is less than 0.05 eV and quite acceptable for our purposes.

TABLE II. Defect formation energy in ZnSe and ZnMgSe, all the energies given are in eV

	Defect	Formation Energy
	$(Cl_{Se})^{0}$	$1.36+\lambda\Delta H$
pure ZnSe	$(Cl_{Se})^{1+}$	$-0.59+\lambda\Delta H+\mu_e$
(32 atom supercell)	$(Cl_{Se}\text{-}V_{Zn})^{1-}$	$2.03-\mu_e$
	$(V_{Zn})^{2-}$	$4.41-\lambda\Delta H-2\mu_e$
	$(Cl_{Se})^{0}$	$1.22+\lambda\Delta H$
$Zn_{0.94}Mg_{0.06}Se$ (one Mg atom located as	$(Cl_{Se})^{1+}$	$-0.82+\lambda\Delta H+\mu_e$
the nearest neighbor of Cl in 32 atom supercell)	$(Cl_{Se}\text{-}V_{Zn})^{1-}$	$1.90-\mu_e$
	$(V_{Zn})^{2-}$	$4.50-\lambda\Delta H-2\mu_e$
	$(Cl_{Se})^{0}$	$1.02+\lambda\Delta H$
$Zn_{0.87}Mg_{0.13}Se$ (two Mg atoms located as	$(Cl_{Se})^{1+}$	$-1.03+\lambda\Delta H+\mu_e$
the nearest neighbors of Cl in 32 atom supercell)	$(Cl_{Se}\text{-}V_{Zn})^{1-}$	$1.75-\mu_e$
	$(V_{Zn})^{2-}$	$4.60-\lambda\Delta H-2\mu_e$
	$(Cl_{Se})^{0}$	$0.91+\lambda\Delta H$
$Zn_{0.81}Mg_{0.19}Se$ (three Mg atoms located as	$(Cl_{Se})^{1+}$	$-1.20+\lambda\Delta H+\mu_e$
the nearest neighbors of Cl in 32 atom supercell)	$(Cl_{Se}\text{-}V_{Zn})^{1-}$	$1.62-\mu_e$
	$(V_{Zn})^{2-}$	$4.72-\lambda\Delta H-2\mu_e$
$Zn_{0.81}Mg_{0.19}Se$ (three Mg atoms located as		
the third neighbors of Cl in 32 atom supercell)	$(Cl_{Se})^{1+}$	$-0.67+\lambda\Delta H+\mu_e$

In addition to the inherent problems associated with the LDA-DFT calculation and potential limitations of a relatively small 32-atom supercell, the uncertainty in the definition of chemical potentials [especially of a chlorine atom (μ_{Cl})] could cause errors in the absolute values of the formation energies given in Table II. However, the main emphasis of this publication is to trace the relative change of the formation energy and thus the pinned Fermi level for ZnMgSe alloys with different Mg contents. The relative changes in these values are much less sensitive to the above mentioned limitations of the calculations, and therefore, much more reliable.

III. EXPERIMENTAL APPROACH

ZnSe thin films were grown in a custom molecular beam epitary (MBE) system at West Virginia University on semi-insulating (100) GaAs substrates using procedures discussed previously.[28] Chlorine-doped ZnSe layers were grown on an undoped 0.35 μm buffer layer with a total thickness of 2 to 2.4 μm at 300°C with a growth rate of $\sim$0.33 μm/h. High-purity elemental zinc, magnesium, and selenium were used from conventional MBE sources. Chlorine doping was achieved using a standard effusion cell with $ZnCl_2$ as source material. Growth occurred under slightly Se-stable conditions determined by monitoring the disappearance of the Zn-stable [010] $c(2\times2)$ reflection high-energy electron diffraction (RHEED) reconstruction.[29] Secondary ion mass spectrometry (SIMS) measurements were made at Charles Evans and Associates (Sunnyvale, CA) to determine the doping concentration profiles of chlorine in ZnSe and $Zn_xMg_{1-x}Se$ samples using Cs^+ ions. Measurements of chlorine in ZnSe and $Zn_xMg_{1-x}Se$ indicated minimum detectabilities of 5×10^{15} and 1×10^{16} cm^{-3}, respectively. Absolute concentrations were determined using a chlorine standard prepared by ion implantation in a thick MBE ZnSe layer. Magnesium percentages were also determined using direct comparison to a ZnMgSe standard whose Mg concentration was determined using x-ray diffraction. Lattice constant measurements were determined using the Bond method with a Si single crystal as a monochromator for x-ray diffraction using Cu $K\alpha_1$ radiation.

Hall measurements were performed using a typical Keithley Instruments Hall effect setup. Indium contacts soldered to the samples were ohmic, and measurements were made using the standard Van der Pauw geometry.

IV. RESULTS AND DISCUSSION

A. Lattice constant in Cl-doped ZnMgSe alloy

The equilibrium lattice constant was found to be 5.628 Å for pure ZnSe. The lattice relaxation around the isolated Cl_{Se}^{1+} defect resulted in an increase by about 6.7% for the four Cl_{Se}-Zn bonds. The relaxation around the $(Cl_{Se}\text{-}V_{Zn})^{1-}$ complex is more complicated. In this complex, the Cl_{Se}-V_{Zn} bond length increases about 3%, the three V_{Zn}-Se bonds decrease about 5% and the three Cl_{Se}-Zn bonds increase less than 2% (see Fig. 1). We would thus expect an overall increase in lattice constant due to significant concentrations of $(Cl_{Se})^{1+}$ centers, and almost no change in lattice constant due to $(Cl_{Se}\text{-}V_{Zn})^{1-}$ complexes. In addition, we calculated the lattice constant of zinc blende ZnCl to be 6.0 Å. Thus, our calculations predict that the addition of Cl will lead to a net increase in lattice constant, while $(Cl_{Se}\text{-}V_{Zn})^{1-}$ complex formation will not contribute to this lattice expansion. The above changes in bond lengths should be treated as lower limits on actual values because of the limitations imposed by using a (relatively limited) finite number of atoms in the calculations.

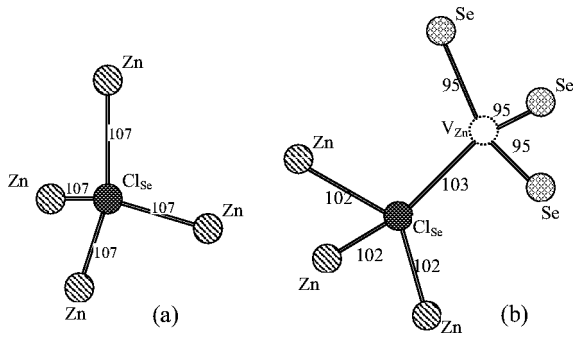

FIG. 1. Lattice relaxation around Cl_{Se}^{1+} and $(Cl_{Se}\text{-}V_{Zn})^{1-}$ complex in ZnSe. The center of the zinc vacancy is defined as the position of a zinc atom in a perfect lattice. The bond lengths are given in percent of the bond length in the ideal lattice. (a) is for the Cl_{Se}^{1+} and (b) is for the $(Cl_{Se}\text{-}V_{Zn})^{1-}$ complex.

Consistent with our predictions, Ohkawa *et al.*[30] showed a dramatic increase in lattice constant with Cl doping in the regime where heavy compensation is not expected. We extended these measurements up to Cl concentrations of 6×10^{19} cm^{-3}, where heavy compensation occurs. We observed a continuing increase in lattice constant for increasing Cl concentration, but at a rate less than that indicated by the data of Ohkawa *et al.* A Vegard-law-type extrapolation for our data indicated a lattice constant of 7.1 Å would occur for Cl occupying 100% of the Se sites, while the data of Ohkawa *et al.*'s data would indicate an even larger value. The continuing increase in lattice constant in compensated material can be understood by the fact that high compensation requires the sample to have a near equal number of $(Cl_{Se})^{1+}$ and $(Cl_{Se}\text{-}V_{Zn})^{1-}$ centers, with the net lattice expansion due to the $(Cl_{Se})^{1+}$ being the dominant effect.

Of interest, an x-ray absorption fine structure measurement on the Cl *K* absorption edge by Maruyama *et al.*[31] found experimental bond lengths of 2.5 and 2.8 Å for Zn nearest neighbors in heavily Cl-doped ZnSe. They assigned the experimental bond length of 2.5 Å to the Cl_{Se}-Zn bond for isolated (Cl_{Se}^{1+}) by assuming the Cl will not significantly perturb the lattice, and thus by default assigned the 2.8 Å bond to the Cl_{Se}-Zn bonds in the $(Cl_{Se}\text{-}V_{Zn})^{1-}$ complex. Our results indicate that the opposite assignment is more likely, with reasonable agreement between our calculated results (2.6 Å for the Cl_{Se}-Zn bond around isolated Cl_{Se}^{1+}, and 2.5 Å for the Cl_{Se}-Zn bonds in the $Cl_{Se}\text{-}V_{Zn}^{1-}$ complex) and the two measured values. Clearly more work is required before a definitive experimental assignment can be made.

The equilibrium lattice constants for ZnSe and ZnMgSe alloys with different Mg content were also calculated. We obtained the following lattice constants 5.628, 5.646, 5.663, and 5.682 Å for pure ZnSe, $Zn_{0.94}Mg_{0.06}Se$, $Zn_{0.87}Mg_{0.13}Se$, and $Zn_{0.81}Mg_{0.19}Se$, respectively. We also calculated the lattice constant of zinc blende structure MgSe, to be 5.921 Å. The calculated lattice constants of ZnSe and MgSe are in good agreement with the experimental values of 5.668 and 5.890 Å for ZnSe and MgSe, respectively. For the ZnMgSe alloy, all these calculated lattice constants follow Vegard's law (See Fig. 2).

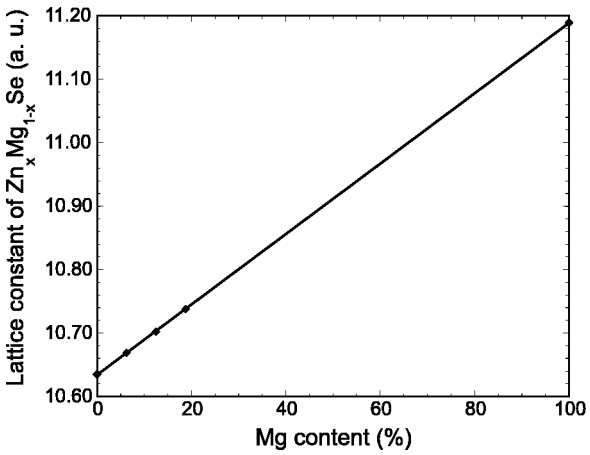

FIG. 2. Lattice constant vs Mg content for $Zn_xMg_{1-x}Se$ alloys. The points (from left to right) in the figure represent the calculated lattice constant for Mg content of 0, 6.25, 12.5, 18.75, and 100 %, respectively. It implies that the lattice constant of $Zn_xMg_{1-x}Se$ alloy agrees with Vegards Law.

B. Mg location in ZnMgSe:Cl alloy

Our calculations indicated that, without the presence of chlorine, magnesium atoms do not have preferential positions in the ZnMgSe alloy. We came to this conclusion after considering two special supercells. While both of them contained three Mg atoms, the spatial configurations of these atoms are very different. In the first supercell, all three Mg atoms are located at sites marked as 3 in Fig. 3. In this geometry, Mg atoms are as close to each other as possible, and they are also the nearest neighbors of the atom at site 2 (this is the site we used for chlorine substitution). In case two, the Mg atoms are located at sites marked 7 in Fig. 3. In this geometry, Mg atoms are one zinc site apart from each other (at the second nearest zinc sites to each other).

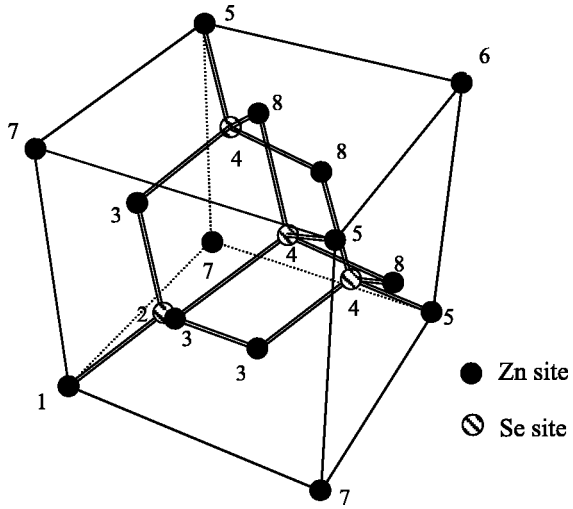

FIG. 3. Structure of ZnSe. To get the preferred locations of Mg atoms, two configurations are considered in $Zn_{0.81}Mg_{0.19}Se$ (three Mg atoms in the 32-atom supercell). The first case has all three Mg atoms at sites marked by 3, and in the second case the Mg atoms are located at sites marked by 7. Site 2 is the position for the substitutional chlorine atom when chlorine is used as a dopant.

In the absence of chlorine, the total energy difference between these two cases is less than 0.05 eV. The first case (all Mg are nearest neighbors) has the lower energy. Since the difference is small (it is about the same order as numerical error in our calculations), we believe there is no site preference for the magnesium atoms. That means the ZnMgSe is a random alloy, rather than an ordered alloy as seen in some other materials such as CuZn and AuCu.[32]

Completely different results were obtained when a selenium atom at site 2 is substituted by a chlorine atom. The total energy of the first supercell (with three Mg atoms as the nearest neighbors of Cl) is 0.57eV lower than for the second supercell (Mg atoms are located at the second nearest zinc sites with respect to Cl). Thus, it is energetically favorable for Cl and Mg to be the nearest neighbors. Therefore, in Table II we considered supercells with geometry where Mg atoms are in positions as nearest neighbors to chlorine atoms. Only one case, when Mg atoms are in the positions as the third nearest neighbors (the second nearest zinc sites) to chlorine atoms, is presented for comparison to illustrate the large difference in total energy.

Qualitatively, the preference of Cl for Mg-rich regions can also be explained by comparing the heat of formation of MgSe (2.93 eV), $MgCl_2$ (6.65 eV), ZnSe (1.65 eV) and $ZnCl_2$ (4.31 eV).[33] The difference in heat of formation between $MgCl_2$ and MgSe is 3.72 eV, and the difference between $ZnCl_2$ and ZnSe is 2.66 eV. Therefore, one can estimate that the energy difference between Mg-Cl and Mg-Se bonds is higher than between Zn-Cl and Zn-Se bonds. When a chlorine atom substitutes for a Se atom in ZnMgSe, it will more likely occupy a Se site with more Mg neighbors, because the resulting Mg-Cl bonds lower the energy of the system. In our case, in the first supercell, as described above, the chlorine atom at site 2 has three Mg atoms and only one Zn atom as nearest neighbors. It is likely that if such an arrangement exists the chlorine will substitute for the selenium atom there and form three Mg-Cl bonds. In supercell two, the chlorine atom would have four Zn atoms as nearest neighbors, and therefore only Zn-Cl bonds are formed. Therefore, this analysis also supports our prediction that chlorine always favors substituting for the selenium atom with more Mg atoms as neighbors, and our calculated 0.57 eV difference is also reasonable in magnitude.

C. Defect formation energies in ZnSe and ZnMgSe

In this paper, we only considered formation energies for the following defects: chlorine substituting for selenium (neutral Cl_{Se}^{0} and single positive charge Cl_{Se}^{1+} states), a zinc vacancy (double negative charge V_{Zn}^{2+} state) and, a $(Cl_{Se}\text{-}V_{Zn})^{1-}$ complex. All formation energies were calculated in pure ZnSe and in $Zn_xMg_{1-x}Se$. Based on prior studies,[7] these are the most pertinent defects for Cl doping in this alloy system.

The calculated formation energies are shown in Table II. From these results, it can be noticed that the change of the formation energies for all the chlorine related defects and complexes strongly depend on the number of Mg atoms that are nearest neighbors to chlorine, instead of the total number of Mg atoms in the supercell (or the Mg content). For example, when compared with pure ZnSe, the formation energy of Cl_{Se}^{1+} decreases 0.23, 0.44, and 0.61 eV for chlorine at a selenium site with one, two, and three Mg atoms as the nearest neighbors, correspondingly. In comparison, this formation energy decreases only 0.08 eV for the chlorine atom with three Mg atoms as the third nearest neighbors (the second nearest zinc sites).

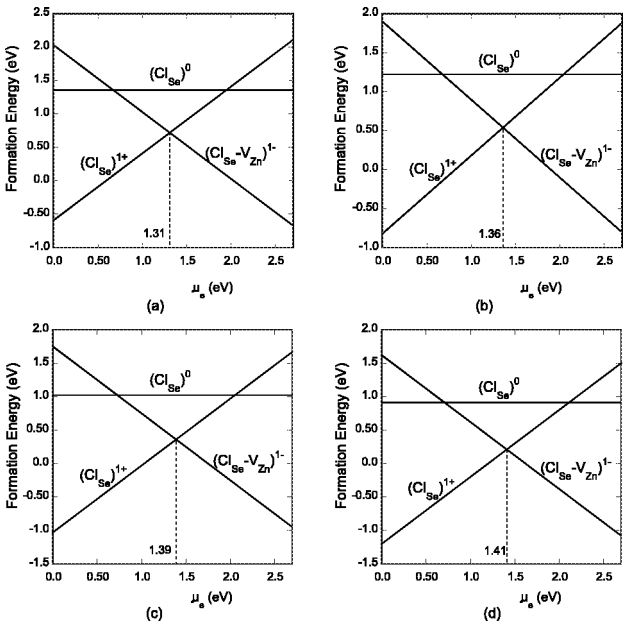

FIG. 4. Formation energies of chlorine related defects in ZnSe and $Zn_xMg_{1-x}Se$ alloys under Zn-rich condition ($\lambda=0$). (a) is for pure ZnSe, (b), (c), and (d) are corresponding to $Zn_xMg_{1-x}Se$ with one, two, or three Mg atoms as the nearest neighbors of chlorine atom, respectively. The Fermi levels are pinned at 1.31, 1.36, 1.39, and 1.41 eV above the valence band for (a), (b), (c), and (d), respectively.

Judging from the results presented in Table II, the change of the formation energy of Cl_{Se}^{1+} has roughly a linear dependence on the number of Mg atoms as the nearest neighbors of Cl. The formation energy for the $(Cl_{Se}\text{-}V_{Zn})^{1-}$ complex follows a similar trend, going down by 0.13, 0.28, 0.41 eV for chlorine at a selenium site with one, two, and three Mg atoms as nearest neighbors to the Cl atom compared with pure ZnSe. These results also suggest the formation energy changes due to the chlorine substituting for the selenium atom in a Mg-Se bond instead of a Zn-Se bond. For the chlorine-substituting-selenium neutral defect $(Cl_{Se})^0$, the formation energy also decreases with the addition of Mg. Therefore, the chlorine solubility should increase dramatically in ZnMgSe (see additional discussion below).

Second, from Table II, we note that, when the number of Mg atoms as nearest neighbors increases, the formation energy of the main compensating complex $(Cl_{Se}\text{-}V_{Zn})^{1-}$ is lowered at a slower rate than the formation energy of Cl_{Se}^{1+}. Therefore, the final pinned Fermi level should be higher in ZnMgSe than in pure ZnSe as measured from the top of the valence band. The formation energy of defects versus μ_e are shown in Fig. 4. Upon considering the two competing effects

(doping vs compensation), we can see that, because of the compensation by $(Cl_{Se}\text{-}V_{Zn})^{1-}$, the Fermi level will be pinned at 1.31, 1.36, 1.39, and 1.41 eV for chlorine doping in ZnSe and $Zn_xMg_{1-x}Se$, which have one, two, and three Mg atoms as the nearest neighbors to chlorine, respectively.

Increase of the maximum achievable μ_e by 0.10 from 1.31 eV for pure ZnSe to 1.41 eV for ZnMgSe (each chlorine atom having three Mg atoms as the nearest neighbors) would be favorable for *n*-type doping, providing that the band gap is the same for the two materials. But the fact that the band gap is also increasing in the presence of magnesium has a dramatic effect, as we discuss later.

We would like to point out that in Fig. 4, we plot the formation energies under zinc-rich conditions ($\lambda=0$). Under different stochiometric conditions (e.g., selenium rich), the formation energy lines for Cl_{Se} move up by $\lambda\Delta H$ (see Table II). Therefore, the formation energy of Cl_{Se} is higher, and the pinned Fermi level moves left (lower). However, neglecting the change in the heat of formation, these shifts are the same for all four cases presented in Fig. 4. Therefore, the main tendency remains the same: the formation energies for Cl_{Se} is lower when there are more Mg atoms as nearest neighbors. To predict the relative trends in the maximum electron concentration, we must also know the dependence of the number of Mg atoms as the nearest neighbors of chlorine on the average Mg content in ZnMgSe.

D. Average number of Mg atoms as the nearest neighbors of Cl

As we discussed, the change of the formation energies for chlorine related defects and the Cl-vacancy complex, as well as the maximum achievable μ_e in ZnMgSe directly depend on the number of Mg atoms that exist as nearest neighbors to chlorine. Therefore, we need to estimate the change in the average number of Mg atoms as nearest neighbors to Cl for ZnMgSe alloy with varying Mg content. For highly Cl-doped ZnMgSe, the Cl concentration can reach $10^{20}/cm^3$ (the zinc site density is about $2.2\times10^{22}/cm^3$ in ZnSe). Therefore, for Mg content as low as 2%, the atom ratio between Mg and Cl is higher than 4:1.

Our results have shown that the magnesium atoms tend to be nearest neighbors of chlorine atoms for the lowest energy configuration. However, this does not mean that each chlorine atom should have exactly four Mg atoms as nearest neighbors, because entropy effects must also be considered here.

To obtain the relationship between the average number of Mg atoms as nearest neighbors of chlorine and the Mg content in $Zn_xMg_{1-x}Se$ we used the following simple model. We consider a small volume inside ZnMgSe:Cl with *m* metal (i.e., Zn or Mg) sites and an equal number of Se sites. For simplicity assume that this is an isolated system and there is only one Cl atom inside it. In the system there are $m-1$ Se atoms at the Se sites and $m-n$ Zn atoms plus *n* Mg atoms at metal sites. For this system, the energy depends only on the number of Mg atoms as chlorine's nearest neighbors (antisite defects are not allowed). Therefore, there are five energy states with total energy of E_0, E_1, E_2, E_3, and E_4, corresponding to zero, one, two, three, and four Mg atoms as chlorine's nearest neighbors. The partition function of this system is equal to

$$Z=\sum_{i=0}^{4} g_i \exp(-\beta E_i),$$

where $g_i=C_4^i C_{m-4}^{n-i}$. From our results in Table II, it can be seen that $E_i\approx E_0-i^*\Delta$, $i=1,2,3,4$; and $\Delta=0.2$ eV.

Using this relationship the average number of Mg atoms as chlorine's nearest neighbors (N) versus Mg content can be calculated as

$$\langle N\rangle=\frac{1}{Z}\sum_{i=0}^{4} i g_i \exp(-\beta E_i).$$

The result is shown in Fig. 5. Note that, for highly Cl-doped ZnMgSe, *m* is in the hundreds. We can see that when the Mg content is about 1%, each chlorine atom on average has only one Mg atom as the nearest neighbor but, when Mg concentration exceeds 8%, there are more than three Mg atoms on average as nearest neighbors for each chlorine atom.

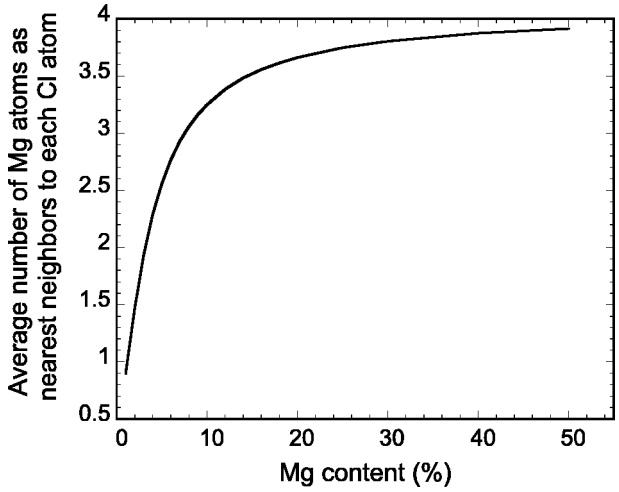

FIG. 5. Average numbers of Mg atoms as the nearest neighbors to each Cl as a function of Mg content in the $Zn_xMg_{1-x}Se$ alloy. The growth temperature of 600 K is used, as it is discussed in the text.

E. Solubility

From the calculated results discussed above, we[34] predicted that the addition of Mg reduces the substitution energy of chlorine for selenium. Therefore, the chlorine incorporation increases with Mg concentration. To directly test this hypothesis, an alloy-modulated structure was grown under a constant $ZnCl_2$ flux. The $ZnCl_2$ oven was fixed at a temperature of 146 °C, which produces a Cl incorporation of 5×10^{18} atoms/cm^{-3} for pure ZnSe. $Zn_xMg_{1-x}Se$ ''steps'' were produced with $(1-x)$ values of 0.16, 0.27, and 0.43 by sequentially opening and closing the Mg shutter in one-hour intervals. The Mg oven temperature was increased while the shutter was closed. The sample was grown on, and capped with, an undoped 0.35 μm ZnSe buffer layer. Chlorine-

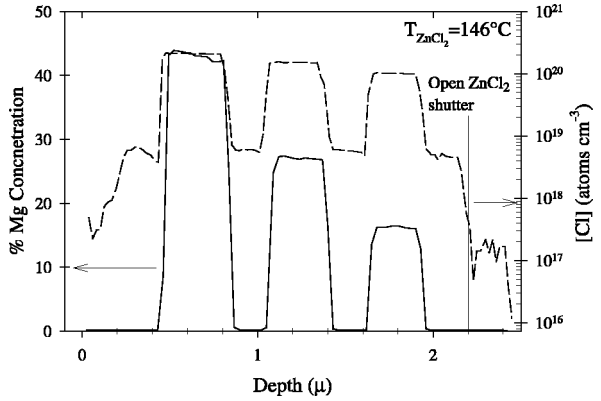

FIG. 6. SIMS profile step alloyed $Zn_xMg_{1-x}Se$ sample. The doping occurred at a constant $ZnCl_2$ oven temperature of 146°C. The alloyed steps have $(1-x)$ values of 0.16, 0.27, and 0.43.

doped ZnSe was grown before, between, and after the steps. The Cl incorporation returned to the same level for each ZnSe:Cl layer, and exhibited a dramatic increase during the steps where Mg was present. The Cl concentration increases less dramatically from step to step because the presence of the Mg levels in the initial step incorporates much of the available Cl. These results, summarized in Figs. 6 and 7, directly confirm the modeling predictions.

However, we should point out that, from our calculation at a Mg content of 8%, the average number of Mg atoms as nearest neighbors of chlorine is three. Including the effect of the change in chemical potential μ_e, the $(Cl_{Se})^{1+}$ formation energy is 0.5 eV lower in $Zn_{0.92}Mg_{0.08}Se$ than in pure ZnSe. This would indicate that at the growth temperature ($\sim$600 K) chlorine incorporation could be higher by roughly 10^4. This again suggests that the current results are limited by the amount of Cl present at the growing surface. It should also be kept in mind that the crystal growth is not a thermodynamically equilibrated process; therefore, one has to be very careful in using formation energy for estimation of the concentrations (or concentration differences) of defects. As we suggested above, the decrease in the formation energy mainly comes from the effect of chlorine replacing the selenium in the Mg-Se bond. When most chlorine atoms already have Mg atoms as neighbors, further increase in Mg content will not decrease that energy dramatically, and the increase in Cl incorporation with increasing Mg will lessen in that case. Thus, one would expect an immediate drastic increase in Cl solubility, followed by the slower increase with increasing Mg as is presented in Fig. 7.

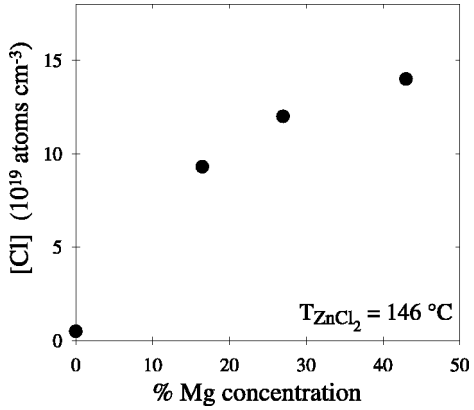

FIG. 7. Experimental chlorine incorporation as a function of Mg content in $Zn_xMg_{1-x}Se$ for a constant Cl flux.

F. Maximum electron concentration

The electron concentration in a semiconductor can be found as

$$n = N_c F_{1/2}[(\mu_e - E_{\text{gap}})/k_B T], \tag{1}$$

where μ_e is the Fermi energy with respect to valence band edge, E_{gap} is the band gap, and N_c is the effective density of states. Using effective mass approximation, N_c is equal to

$$N_c = 2\left(\frac{m^* k_B T}{2\pi\hbar^2}\right)^{3/2} \tag{2}$$

and $F_{1/2}(\eta)$ is the Fermi integral

$$F_{1/2}(\eta) = \frac{2}{\sqrt{\pi}}\int_0^\infty \frac{u^{1/2}du}{\exp(u-\eta)+1}. \tag{3}$$

For $Zn_xMg_{1-x}Se$ with different Mg content, we ignore the change in effective mass m^*, so N_c is a constant at a given temperature in this approximation. Therefore, to predict the change in the maximum electron concentration in $Zn_xMg_{1-x}Se$:Cl with different Mg content, we need to know the changes in maximum achievable Fermi level μ_e and band gap E_{gap}, which both depend on the Mg content in ZnMgSe alloy. The change in the band gap can be approximated[14] as

$$E_{\text{gap}} = xE_{\text{gap}}^{\text{ZnSe}} + (1-x)E_{\text{gap}}^{\text{MgSe}} - cx(1-x), \tag{4}$$

where $c = 0.1$ eV is the bowing parameter of a ZnMgSe alloy.

The change in the maximum achievable Fermi level μ_e depends primarily on the number of Mg atoms as the nearest neighbor of chlorine (see Fig. 4). We can also obtain the average number of Mg atoms as nearest neighbors to each chlorine atom for $Zn_xMg_{1-x}Se$ with different Mg content from the calculations shown in Fig. 5. Therefore, by using the results shown in Figs. 4 and 5, we can reasonably estimate the change of μ_e in $Zn_xMg_{1-x}Se$ with different Mg content and thus predict the trends in maximum electron concentration.

Comparison of our predicted trend with the experimental results of Ferreira *et al.*[15] is shown in Fig. 8. We have to point out that the band gap and absolute values of the pinned

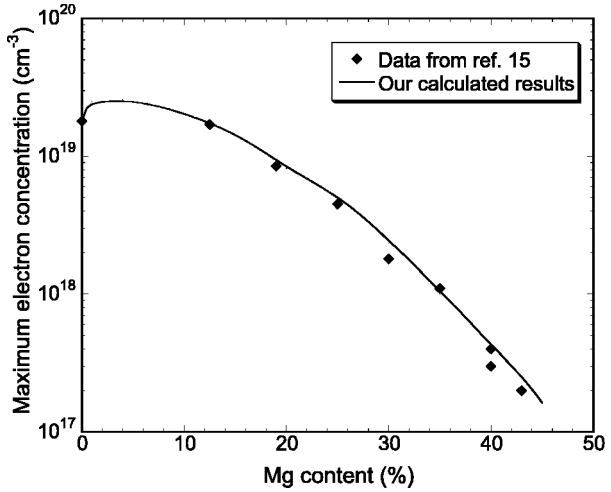

FIG. 8. Maximum achievable electron concentration as a function of Mg content in the $Zn_xMg_{1-x}Se$ alloy.

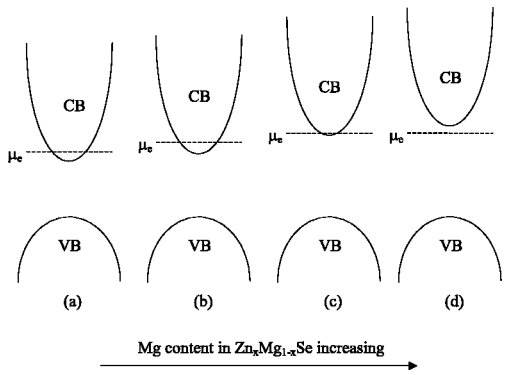

FIG. 9. Schematic of the change in bandgap and Fermi level in $Zn_xMg_{1-x}Se$ alloy with increasing Mg content. For (a) $(1-x)=0$, (b) $(1-x)<5\%$, (c) $(1-x)\sim 5$–$20\,\%$, and (d) $(1-x)>20\%$. The experimental value of $E_{\rm gap}$ adjusted for Mg concentration [see Eq. (4)]. Calculated pinned Fermi levels μ_e are shifted by a constant to reproduce the experimental value for pure ZnSe.

Fermi level μ_e cannot be accurately calculated in our model because of the LDA's failure in predicting the band gap of semiconductors. However, we think that the relative change of μ_e is reliably calculated. Therefore in the calculation of the electron concentration, we use the experimental data for pure ZnSe to get μ_e (about 130 meV above the bottom of conduction band) in ZnSe, and then calculate changes to obtain the corresponding μ_e for $Zn_xMg_{1-x}Se$ for different x. Specifically, we calculated three points with Mg content of 1, 4, and 8 %. These concentrations correspond to one, two, and three Mg atoms as nearest neighbors to each chlorine atom (see Fig. 5), with the corresponding shift of μ_e equal to 50, 80, 100 meV (see Fig. 4). For Mg content larger than 20% , as shown in Fig. 5, the number of Mg atoms surrounding each chlorine atom is essentially 4. Above this concentration, we thus use a constant shift in μ_e of 110 meV, obtained by simple extrapolation from previous calculations. The calculated results are shown as the solid line in Fig. 8.

The growth temperature of $\sim$600 K was used in the calculation of the maximum electron concentration calculation for ZnMgSe, resulting in extremely good agreement with the experimental results. The growth temperature must be used since the number of donors (N_d) and the number of acceptors (N_a) are determined during the growth and remain fixed afterwards. For fully ionized donors, as would be expected for the low thermal ionization energy of Cl in this system (and especially in the degenerate case), electron concentration ($n=N_d-N_a$) will not change significantly when the temperature is reduced from the growth temperature ($\sim$600 K) to room temperature ($\sim$300 K). This situation suggests that by increasing the growth temperature the electron concentration can also be increased.

From Eq. (1), it follows that the maximum electron concentration depends only on the difference between μ_e and $E_{\rm gap}$ at a given temperature. The change in Fermi level μ_e and bandgap $E_{\rm gap}$ (experimental value used) are both depicted schematically in Fig. 9. Panel (a) shows pure ZnSe. Panel (b) describes a small amount of Mg ($<5\%$). Increasing numbers of Mg atoms around each chlorine atom causes the μ_e to grow faster than the increase in $E_{\rm gap}$, which leads to higher electron concentration. When more Mg is added [5–20 % as shown in panel (c) of Fig. 9], the increase in μ_e is now much smaller than the change in bandgap, and the carrier concentration begins to fall. The situation with large Mg content ($>20\%$) is shown in panel (d). Because most of the chlorine atoms are already surrounded by Mg atoms, μ_e changes little, and the increase in the bandgap becomes the dominant factor. Therefore, the carrier concentration drops dramatically for large Mg content. Calculations show that, for small Mg content (around 5%), the maximum achievable electron concentration for the $Zn_xMg_{1-x}Se$ alloy system might be reached. However, it is only about 40% more than that for pure ZnSe, a difference that may prove difficult to be confirmed by experiments.

V. CONCLUSION

We have shown that in chlorine-doped ZnMgSe alloy system, chlorine has a strong tendency to substitute on selenium sites that are surrounded by Mg atoms. The formation energies for the chlorine-substituting for-selenium defects and the chlorine-substituting-for-selenium with neighboring zinc-vacancy defect complex all decrease with increasing Mg content. This decrease leads to higher chlorine incorporation in $Zn_xMg_{1-x}Se$ alloy with higher Mg content. Our most recent MBE experiments clearly show this increased chlorine solubility in $Zn_xMg_{1-x}Se$ alloys. However, with the presence of magnesium, the decrease of the formation energy of the compensating defect $(Cl_{Se}\text{-}V_{Zn})^{1-}$ coupled with the increase in band gap leads to a lower achievable electron compensation. Thus, the net effect of adding magnesium to ZnSe is a decrease in the maximum achievable electron concentration when chlorine is used as an *n*-type dopant.

ACKNOWLEDGMENTS

This research was supported by National Science Foundation Grant No. DMR-98-06299.

[1] S. Nakamura, M. Senoh, S. Nagahama, N. Jwasa, T. Yamada, T. Matsushita, H. Kiyoku, Y. Sugimoto, T. Kozaki, H. Umemoto, M. Sano, and K. Chocho, Jpn. J. Appl. Phys., Part 2 **37**, L309 (1998).
[2] D. B. Laks, C. G. Van-de-Walle, G. F. Neumark, and S. T. Pantelides, Phys. Rev. Lett. **66**, 648 (1991).
[3] A. Garcia and J. E. Northrup, Phys. Rev. Lett. **74**, 1131 (1995).
[4] C. G. Van-de-Walle, D. B. Laks, G. F. Neumark, and S. T. Pantelides, Phys. Rev. B **47**, 9425 (1993).
[5] Byoung-Ho-Cheong, C. H. Park, and K. J. Chang, Phys. Rev. B **51**, 10 610 (1995).
[6] C. H. Park and D. J. Chadi, Phys. Rev. Lett. **75**, 1134 (1995).
[7] S. Pöykkö, M. J. Puska, and R. M. Nieminen, Phys. Rev. B **57**, 12 164 (1998).
[8] S. Pöykkö, M. J. Puska, and R. M. Nieminen, Phys. Rev. B **57**, 12 174 (1998).
[9] S. Gundel, D. Albert, J. Nürnberger, and W. Faschinger, Phys. Rev. B **60**, R16 271 (1999).
[10] K. Saarinen, T. Laine, K. Skog, J. Mäkinen, P. Hautojärvi, K. Rakennus, P. Uusimaa, A. Salokatve, and M. Pessa, Phys. Rev. Lett. **77**, 3407 (1996).
[11] K. M. Yu, J. W. AgerIII, E. D. Bourret, and W. Walukiewicz, J. Appl. Phys. **75**, 1378 (1994).
[12] K. Akimoto, T. Ogawa, T. Maruyama, and Y. Kitajima, J. Cryst. Growth **159**, 350 (1996).
[13] F. C. Peiris, S. Lee, U. Bindley, and J. K. Furdnya, J. Appl. Phys. **86**, 918 (1999).
[14] H. Okuyama, Y. Kishita, and A. Ishibashi, Phys. Rev. B **57**, 2257 (1998).
[15] S. O. Ferreira, H. Sitter, and W. Faschinger, Appl. Phys. Lett. **66**, 1518 (1995).
[16] H. Krakauer and B. R. Cooper, Phys. Rev. B **16**, 605 (1977); C. Q. Ma, M. V. Ramana, B. R. Cooper, and H. Krakauer, *ibid.* **34**, 3854 (1986).
[17] J. M. Wills and B. R. Cooper, Phys. Rev. B **36**, 3809 (1987).
[18] D. L. Price and B. R. Cooper, Phys. Rev. B **36**, 3809 (1987).
[19] D. L. Price, J. M. Wills, and B. R. Cooper, Phys. Rev. B **46**, 11 368 (1992).
[20] J. M. Wills, O. Eriksson, M. Alouani, and D. L. Price, in *Electronic Structure and Physics Properties of Solids*, edited by H. Dreysse (Springer-Verlag, Berlin, 2000), pp. 148–167.
[21] D. M. Ceperley and B. J. Alder, Phys. Rev. Lett. **45**, 566 (1980).
[22] J. P. Perdew and A. Zunger, Phys. Rev. B **23**, 5048 (1981).
[23] R. Yu, D. Singh, and H. Krakauer, Phys. Rev. B **43**, 6411 (1991).
[24] G. Makov and M. C. Payne, Phys. Rev. B **51**, 4014 (1995).
[25] L. Muratov, S. Little, Y. Yang, B. R. Cooper, T. H. Myers, and J. M. Wills, Phys. Rev. B **64**, 035206 (2001).
[26] L. Heidin and S. Lundqvist, *Solid State Physics*, edited by H. Ehrenreich, F. Seitz, and D. Turnbull (Academic, New York, 1969), Vol. 23, p. l.
[27] A. Fleszar, Phys. Rev. B **64**, 245204 (2001).
[28] Z. Yu, S. L. Buczkowski, N. C. Giles, and T. H. Myers, Appl. Phys. Lett. **69**, 82 (1996).
[29] H. H. Farrell, J. L. deMiguel, and M. C. Tamargo, J. Appl. Phys. **65**, 4084 (1989).
[30] K. Ohkawa, T. Mitsuyu, and O. Yamazaki, J. Appl. Phys. **62**, 3216 (1987).
[31] T. Maruyama, T. Ogawa, K. Akimoto, and Y. Kitajima, Solid State Commun. **103**, 452 (1998).
[32] B. D. Cullity, *Elements of X-ray Diffraction*, 2nd edition (Addison-Wesley, Reading, 1978), pp. 389–391.
[33] O. Kubaschewski and C. B. Alcock, *Metallurgical Thermochemistry* (Pergamon, Oxford, 1979).
[34] Y. Yang, L. Muratov, B. R. Cooper, T. H. Myers, and J. M. Wills, *Advances in Materials Theory and Modeling–Bridging Over Multiple-Length and Time Scales*, MRS Proceedings No. 677 (Materials Research Society, Warrendale, 2001).